Special stability advantages of position-Verlet over velocity-Verlet in multiple-time step integration

Paul F. Batcho[a] and Tamar Schlick[b]
Department of Chemistry and Courant Institute of Mathematical Sciences, New York University and the Howard Hughes Medical Institute, 251 Mercer Street, New York, New York 10012

(Received 13 February 2001; accepted 13 June 2001)

We present an analysis for a simple two-component harmonic oscillator that compares the use of position-Verlet to velocity-Verlet for multiple-time step integration. The numerical stability analysis based on the impulse-Verlet splitting shows that position-Verlet has enhanced stability, in terms of the largest allowable time step, for cases where an ample separation of time scales exists. Numerical investigations confirm the advantages of the position-Verlet scheme when used for the fastest time scales of the system. Applications to a biomolecule, a solvated protein, for both Newtonian and Langevin dynamics echo these trends over large outer time-step regimes. © *2001 American Institute of Physics.* [DOI: 10.1063/1.1389855]

I. INTRODUCTION

The simulation of physical systems with a wide range of temporal and spatial scales poses a considerable challenge to the computational scientist. In the field of biomolecular dynamics, the bonded forces that maintain the molecular structure are vibrational in character, with associated motion time scales on the order of 10^{-14} s (10 fs). However, the long-range electrostatic components and large-scale biomolecular motions, such as protein folding, are characterized by time scales of seconds, many times greater than those of the local bonded forces of the molecule. The first class of numerical algorithms designed to integrate Hamiltonian dynamics were single-time-step (STS) explicit Verlet integrators; these enjoy excellent conservation properties from their symplectic character.[1] Still, such STS schemes limit the time step to a fraction of the fast period of the system (e.g., ≈ 1 fs).

Recently, numerical algorithms designed to integrate larger biomolecular dynamic systems have been introduced in the form of multiple-time-step (MTS) integrators.[2–14] These offer a significant speedup[15] but require care to avoid numerical artifacts such as resonance.[5,16] Work continues on developing methods for longer-time and larger-scale simulations of biological systems.[17–19]

Here, we offer a theoretical analysis that compares the usage of the velocity-Verlet (VV) versus the position-Verlet (PV) scheme for the fastest forces in impulse-Verlet MTS integrators. In the context of MTS formulations based on the symmetric Trotter factorization,[9,12–14] the velocity-Verlet algorithm has been generally used for the fastest (inner) cycle of the MTS integrator. However, we have recently found that PV works better in practice[15] and sought an analytical explanation.

Already, PV for the inner cycle has been advocated by Schlick and co-workers in the context of nonsymplectic stochastic Langevin integrators within the LN-MTS protocol for biomolecular simulations.[4,6,16] The use of extrapolation combined with Langevin dynamics succeeds in damping the resonant impulses inherent in the symplectic MTS integrations and allows enhanced outer time steps, with maintained stability and conservation of energies.[20] The LN approach has demonstrated stable outer time steps up to 120 fs, versus $\sim$4 fs for RESPA type methods; see the companion paper[15] for more details on application of such methods.

Here we analyze PV and VV algorithms when used for the fastest time scale in the MTS integrators. We present a theoretical analysis for a Newtonian–based impulse Verlet integrator of a simple linear system and verify the findings through a nonlinear application to a solvated protein system modeled by the AMBER force field.[15,21,22] The results indicate enhanced stability in the outer time step for the PV version. Besides the LN applications, better conservation properties for PV have been noted[13] when MTS-PV and MTS-VV schemes were applied at larger time steps. Here we delineate the advantages of the PV approach through a detailed theoretical analysis and a biomolecular application; see also our companion paper.[15]

In Sec. II we present the theoretical study of the impulse-Verlet integrator and establish that PV offers enhanced stability for multicomponent harmonic motions with separated time scales. In Sec. III we present results of a MTS integration for a solvated protein and present Newtonian results for large outer-time step integrations. We summarize in Sec. IV the results and discuss future directions of study.

II. LINEAR MODEL FOR MTS ANALYSIS

The analysis of fully nonlinear systems[5,23,24] often begins with linear approximations. For biomolecular simulations, the fastest forces are modeled as harmonic oscillations. Here, we consider the one-dimensional (1D) linear harmonic problem used by Barth and Schlick[6,16]

[a]Electronic mail: paul@biomath.nyu.edu
[b]Author to whom correspondence should be addressed. Fax: 212-995-4152. Electronic mail: schlick@nyu.edu

$$\frac{dX}{dt}=V, \tag{1a}$$

$$\frac{dV}{dt}=-(\lambda_1+\lambda_2)X, \tag{1b}$$

where the variables X and V denote the scalar position and velocity, respectively, for a particle of unit mass. The system can be considered a harmonic oscillator driven by a linear force with constant $\Lambda=\lambda_1+\lambda_2$. Here we study cases where $\lambda_1>\lambda_2$ and study MTS protocols for the two harmonic components when differing in time scales.

The characteristic angular frequencies associated with the two components as well as the total motion are, respectively,

$$\omega_1=\sqrt{\lambda_1}, \quad \omega_2=\sqrt{\lambda_2}, \quad \Omega=\sqrt{\Lambda}. \tag{2}$$

The associated characteristic periods are thus,

$$T_1=\frac{2\pi}{\omega_1}, \quad T_2=\frac{2\pi}{\omega_2}, \quad T=\frac{2\pi}{\Omega}, \tag{3}$$

where T_1 represents the fast motion and T_2 the slower.

A. Linear resonance for impulse-Verlet splitting

Several theoretical studies have been made for impulse-Verlet (IV) algorithms, as well as their mollified versions, in order to gain insight into the large-time step problem.[4,6,7,10,11,16] Barth and Schlick[6,16] examined MTS schemes based on the first-order symplectic Euler method, and Sandu and Schlick[4] analyzed several different MTS schemes based on the second-order Verlet scheme. Here we analyze the stability of the symplectic impulse-Verlet splitting for both VV and PV when used in the inner cycle of a symmetric factorization. The analysis follows that of Ref. 4 for VV.

We start with a two-level splitting of harmonic oscillators in an impulse-MTS scheme where the slow force component $(-\lambda_1 X)$ is evaluated at time steps Δt that are k times larger than those $(\Delta\tau)$ used for the fast component $(-\lambda_2 X)$, i.e., $k=\Delta t/\Delta\tau$. The impulse-MTS scheme with a PV inner cycle becomes

$$X^{[0]}=X^n$$

$$V^{[0]}=V^{[n]}-\frac{k\Delta\tau}{2}\lambda_2 X^{[n]}.$$

$$\left[\begin{array}{l}\textbf{For } i=0:k-1\\ \quad X^{[i+1/2]}=X^{[i]}+\dfrac{\Delta\tau}{2}V^{[i]}\\ \quad V^{[i+1]}=V^{[i]}-\Delta\tau\lambda_1 X^{[i+1/2]}\\ \quad X^{[i+1]}=X^{[i+1/2]}+\dfrac{\Delta\tau}{2}V^{[i+1]}\\ \textbf{end}\end{array}\right]$$

$$X^{[n+1]}=X^k,$$

$$V^{[n+1]}=V^{[k]}-\frac{k\Delta\tau}{2}\lambda_2 X^{[k]}.$$

The VV formulation involves a modification to the inner cycle, bracketed above, as follows:

For $i=0:k-1$

$$V^{[i+1/2]}=V^{[i]}-\frac{\Delta\tau}{2}\lambda_1 X^{[i]},$$

$$X^{[i+1]}=X^{[i]}+\Delta\tau V^{[i+1/2]},$$

$$V^{[i+1]}=V^{[i+1/2]}-\frac{\Delta\tau}{2}\lambda_1 X^{[i+1]}.$$

end

Here the superscripts in brackets denote the indices of the inner iterations. One step of this method advances the solution from $n(k\Delta\tau)$ to $(n+1)(k\Delta\tau)$.

To express the associated propagation matrix A_{IV} for impulse-Verlet, we first introduce the "impulse" matrix

$$P_{\mathrm{IV}}(\Delta\tau,\lambda_2,k)=\begin{bmatrix}1 & 0\\ -\dfrac{k\Delta\tau}{2}\lambda_2 & 1\end{bmatrix}.$$

The propagation matrix of the impulse-Verlet scheme for PV can then be expressed as

$$A_{\mathrm{IV,PV}}(\Delta\tau,\lambda_1,\lambda_2,k)=P_{\mathrm{IV}}(\Delta\tau,\lambda_2,k)A_{\mathrm{PV}}(\Delta\tau,\lambda_1)^k P_{\mathrm{IV}}(\Delta\tau,\lambda_2,k), \tag{4}$$

where

$$\begin{bmatrix}X^{[i+1]}\\ V^{[i+1]}\end{bmatrix}=A_{\mathrm{IV,PV}}\begin{bmatrix}X^{[i]}\\ V^{[i]}\end{bmatrix}, \tag{5}$$

and A_{PV} is the propagation matrix of the PV discretization,

$$A_{\mathrm{PV}}(\Delta\tau,\lambda_1)=\begin{bmatrix}1 & \dfrac{\Delta\tau}{2}\\ 0 & 1\end{bmatrix}\begin{bmatrix}1 & 0\\ -\Delta\tau\lambda_1 & 1\end{bmatrix}\begin{bmatrix}1 & \dfrac{\Delta\tau}{2}\\ 0 & 1\end{bmatrix}.$$

We now introduce the transformation,

$$\cos\,\theta=1-\frac{\Delta\tau^2}{2}\lambda_1, \tag{6}$$

and examine the effective angular frequency in the small time step limit,[4]

$$\theta(\Delta\tau,\lambda_1)=\Delta\tau\omega^{\mathrm{eff}}+\mathcal{O}(\Delta\tau^4). \tag{7}$$

Likewise, consider the large inner-time step limit, that is, $\Delta\tau$ close to the single-time step Verlet stability condition, or $\Delta\tau\leqslant\Delta\tau_s=2/\sqrt{\lambda_1}$,

$$\Delta\tau=2(1-\epsilon)/\sqrt{\lambda_1}, \quad \epsilon>0, \tag{8}$$

where ϵ is a small positive number. In this limit of $\Delta\tau$, we have

$$\cos(\theta)=1-\frac{\Delta\tau^2}{2}\lambda_1\approx -1+4\epsilon+\mathcal{O}(\epsilon^2). \tag{9}$$

For small ϵ this leads directly to

$$\theta \approx \pi(2n+1) + \sqrt{8}\epsilon^{1/2} + \mathcal{O}(\epsilon), \quad \epsilon \ll 1, \quad n = 0,1,2\ldots. \tag{10}$$

For convenience of analysis we also introduce the matrix

$$G_{\mathrm{PV}}(\Delta\tau,\lambda_1) = \begin{bmatrix} 1 & 0 \\ 0 & \dfrac{\sqrt{\lambda_1}}{\sqrt{1-\dfrac{\Delta\tau^2}{4}\lambda_1}} \end{bmatrix},$$

and recast A_{PV} into

$$A_{\mathrm{PV}}(\Delta\tau,\lambda_1) = G_{\mathrm{PV}}(\Delta\tau,\lambda_1) \times \begin{bmatrix} \cos\theta & \sin\theta \\ -\sin\theta & \cos\theta \end{bmatrix} G_{\mathrm{PV}}(\Delta\tau,\lambda_1)^{-1}.$$

We now omit the arguments of A_{PV} and G_{PV} for simplicity. The above transformation clarifies the similarity of A_{PV} to a rotation matrix.

It is also noteworthy to compare the VV inner cycle results, A_{VV} to A_{PV} under the same transformation, namely

$$G_{\mathrm{PV}} = G_{\mathrm{VV}}^{-1} \begin{bmatrix} 1 & 0 \\ 0 & \lambda_1 \end{bmatrix},$$

where

$$G_{\mathrm{VV}} = \begin{bmatrix} 1 & 0 \\ 0 & \sqrt{\lambda_1\left(1-\dfrac{\Delta\tau^2}{4}\lambda_1\right)} \end{bmatrix}.$$

Given that both VV and PV have propagation matrices that are similar to the same rotation matrix, we expect that the linear stabilities will be closely related in the small $\Delta\tau$ limit. *The limit considered in this paper, where PV appears advantageous, occurs instead for large $\Delta\tau$, near the stability limit.*

B. MTS stability analysis

Thus far we have described propagation matrices for a STS Verlet implementation. We proceed with the impulse-MTS analysis following Sandu and Schlick.[4] We define

$$\theta = \theta(\Delta\tau,\lambda_1) = \arccos(1-\Delta\tau^2\lambda_1/2), \tag{11}$$

and temporarily drop the arguments of P_{IV} and G_{IV} for simplicity. The impulse-Verlet propagator can, therefore, be written as

$$\begin{aligned} A_{\mathrm{IV,PV}}(\Delta\tau,\lambda_1,\lambda_2,k) &= P_{\mathrm{IV}}\left(G_{\mathrm{PV}} \begin{bmatrix} \cos(\theta) & \sin(\theta) \\ -\sin(\theta) & \cos(\theta) \end{bmatrix} G_{\mathrm{PV}}^{-1} \right)^k P_{\mathrm{IV}} \\ &= P_{\mathrm{IV}} G_{\mathrm{PV}} \begin{bmatrix} \cos(k\theta) & \sin(k\theta) \\ -\sin(k\theta) & \cos(k\theta) \end{bmatrix} G_{\mathrm{PV}}^{-1} P_{\mathrm{IV}}. \end{aligned} \tag{12}$$

After some algebraic manipulation we have

$$\det(A_{\mathrm{IV,PV}}) = 1, \tag{13}$$

$$\mathrm{trace}(A_{\mathrm{IV,PV}}) = 2\cos(k\theta) - \frac{\lambda_2 k\Delta\tau}{\sqrt{\lambda_1}}\sqrt{1-\frac{\Delta\tau^2}{4}\lambda_1}\sin(k\theta). \tag{14}$$

For the VV version we have

$$\det(A_{\mathrm{IV,VV}}) = 1 \tag{15}$$

$$\mathrm{trace}(A_{\mathrm{IV,VV}}) = 2\cos(k\theta) - \frac{\lambda_2 k\Delta\tau}{\sqrt{\lambda_1\left(1-\dfrac{\Delta\tau^2}{4}\lambda_1\right)}}\sin(k\theta). \tag{16}$$

We now let $*$ denote either V or P for the velocity- or position-Verlet scheme, respectively. We rewrite $\mathrm{trace}(A_{\mathrm{IV},*\mathrm{V}})$ as

$$\mathrm{trace}(A_{\mathrm{IV},*\mathrm{V}}) = 2\cos(k\theta) - 2k\alpha\,\sin(k\theta),$$

where α is method dependent. Namely for VV and PV, α becomes

$$\alpha_{\mathrm{VV}} = \frac{\Delta\tau\lambda_2}{2\sqrt{\lambda_1\left(1-\dfrac{\Delta\tau^2}{4}\lambda_1\right)}}, \tag{17a}$$

$$\alpha_{\mathrm{PV}} = \frac{\Delta\tau\lambda_2\sqrt{1-\dfrac{\Delta\tau^2}{4}\lambda_1}}{2\sqrt{\lambda_1}}. \tag{17b}$$

From our definition of the propagation matrix, Eq. (5), we see that stability is defined by the complex eigenvalues of $A_{\mathrm{IV},*\mathrm{V}}$; namely, if the eigenvalues are on the unit circle then the scheme is stable and if their magnitude exceeds 1 then the scheme is unstable. Since the determinant is 1, both eigenvalues lie on the unit circle (complex conjugates). Instability occurs when the imaginary part goes to zero and both eigenvalues are real, one being either greater than 1 or less than -1; this instability condition results in $\mathrm{trace}(A_{\mathrm{IV},*\mathrm{V}}) > 2$ and $\mathrm{trace}(A_{\mathrm{IV},*\mathrm{V}}) < -2$, respectively. This is also defined as the condition for resonance to occur. For the STS-VV scheme, stability is thus achieved for time step[16]

$$\Delta t \leqslant 2/\sqrt{\lambda_1}. \tag{18}$$

STS-PV can be shown to have the same stability limit. Therefore, the conditions for resonance and stability are the same for the harmonic oscillator and occur when the pair of complex conjugate eigenvalues (lying on the unit circle) becomes a real pair, i.e.,

$$|\mathrm{trace}(A_{\mathrm{IV},*\mathrm{V}})| > 2.$$

More generally, for definitions and examples of resonance see Refs. 4, 6, 7, 25, and 26.

Two cases exist for resonance to occur, namely $\mathrm{trace}(A_{\mathrm{IV},*\mathrm{V}}) < -2$ and $\mathrm{trace}(A_{\mathrm{IV},*\mathrm{V}}) > 2$; in the small $\Delta\tau$ limit, the former can be shown to occur near odd multiples of the fast half period and the latter near integer multiples of the effective fast period. We examine this in more detail below.

First we present the magnitude of the eigenvalues of the propagation matrix A_{IV} for the PV and VV schemes. In Fig.

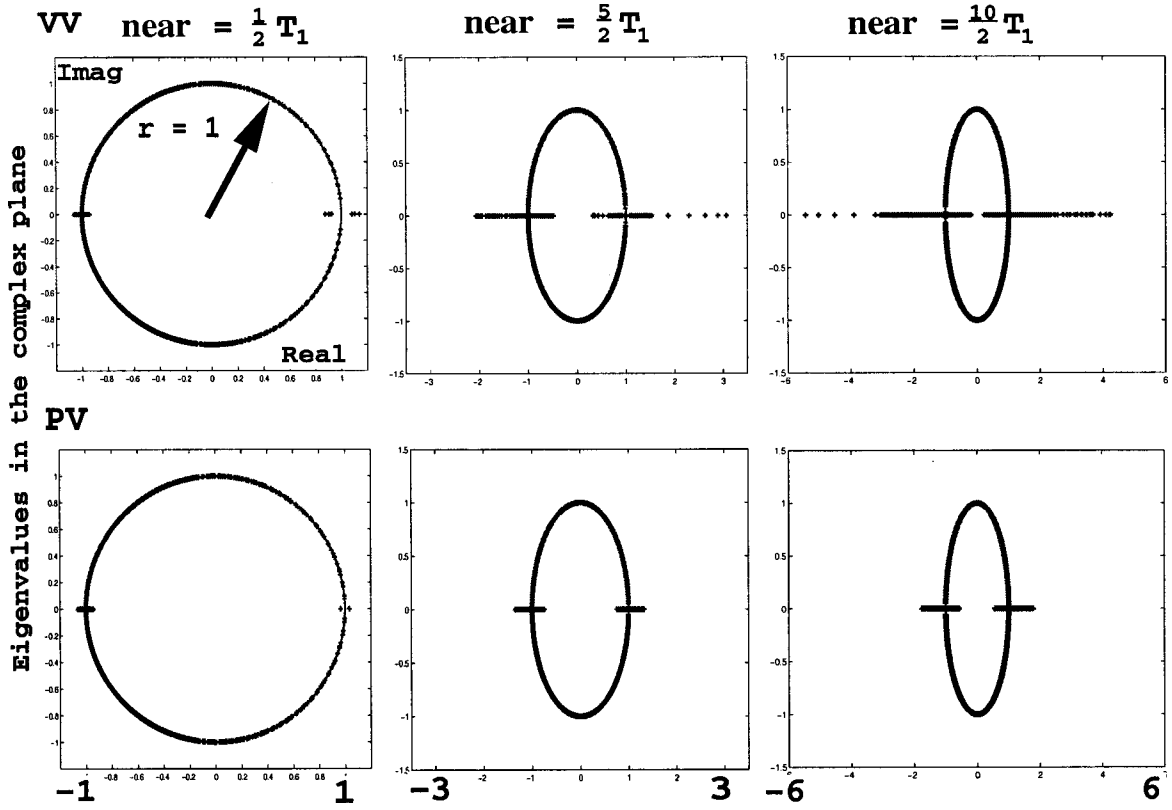

FIG. 1. The eigenvalues for the propagation matrix of a two-component harmonic oscillator are plotted in the complex plane for the position-Verlet (PV) and velocity-Verlet (VV) impulse splitting. The two time periods are $T_1=2$ and $T_2=10$ and the eigenvalues are computed around the half periods of the fast component: $\beta T_1-0.3\leqslant\Delta t\leqslant\beta T_1+0.3$ where $\beta=\frac{1}{2},\frac{5}{2},\frac{10}{2}$; the inner time step $\Delta\tau$ was evaluated in all cases in the range $\Delta t/200\leqslant\Delta\tau\leqslant\Delta t/2$.

1 we examine eigenvalues for the two-component harmonic oscillator in the complex plane for PV and VV impulse splitting. The two time periods are $T_1=2$ and $T_2=10$, and the eigenvalues are computed around three multiples of the half period of the fast component, $\beta T_1-0.3\leqslant\Delta t\leqslant\beta T_1+0.3$ where $\beta=1/2,5/2,10/2$; the inner time step $\Delta\tau$ was evaluated at all values in the range $\Delta t/200\leqslant\Delta\tau\leqslant\Delta t/2$. The global character of the magnitude of the eigenvalues, or more importantly its deviation from the unit circle (resonant spikes), is substantially smaller for the PV scheme. For the $\Delta t=5T_1=10$ resonance case, the VV resonant spikes are approximately three times larger for the examined range of $\Delta\tau$.

Next we study in Fig. 2 the resonant spikes for a relatively small $\Delta\tau=0.01$ and a large $\Delta\tau=0.6$, close to the Verlet stability limit of $\Delta\tau_s=2/\sqrt{\lambda_1}=0.6366$. We see the resonance at multiples of the half period in the small $\Delta\tau$ limit in the top figure and the enhanced stability of PV in the large $\Delta\tau$ limit in the bottom figure. We present an asymptotic analysis below which led us to investigate this large $\Delta\tau$ limit.

C. Asymptotic analysis

We now examine the two cases for instability to occur, namely $\text{trace}(A_{\text{IV},*\text{V}})<-2$ and $\text{trace}(A_{\text{IV},*\text{V}})>2$. An asymptotic analysis is provided for PV and VV in the small inner-time step limit that follows the work in Ref. 4. We then examine the large inner-time step limit and offer calculations that demonstrate the advantages of PV over VV in the neighborhood of $\Delta\tau$ approaching its stability limit.

1. Case I: trace($A_{IV,*V}$)<−2

The condition $\text{trace}(A_{\text{IV},*\text{V}})<-2$ is equivalent to

$$1+\cos(k\theta)-k\alpha\,\sin(k\theta)$$
$$=2\cos^2\left(\frac{k\theta}{2}\right)-2k\alpha\,\sin\left(\frac{k\theta}{2}\right)\cos\left(\frac{k\theta}{2}\right)<0$$

and states that an instability occurs for

$$\tan\left(\frac{k\theta}{2}\right)>\frac{1}{k\alpha}$$

or

$$k\alpha\,\tan\left(\frac{k\theta}{2}\right)>1. \tag{19}$$

Following the analysis in Ref. 4, we note that $\tan(k\theta/2)\rightarrow+\infty$ when

$$\frac{k\theta}{2}\approx(2m+1-\beta)\frac{\pi}{2},\quad m=0,1,2,\ldots,$$

(with β denoting a positive small number and m is an integer). Substituting the relation for the effective angular frequency at small time step, Eq. (7), into the above expression we have

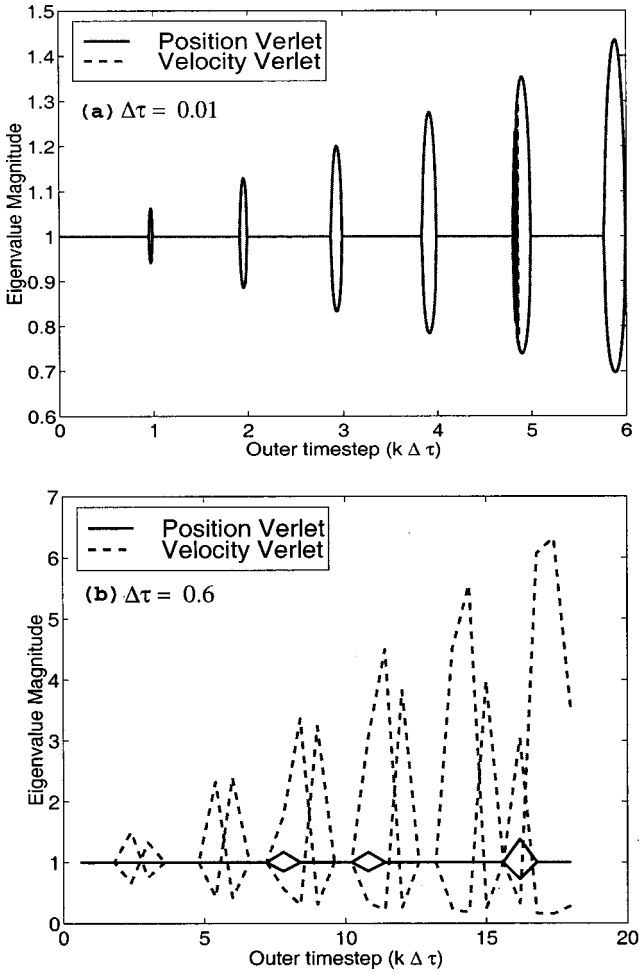

FIG. 2. The magnitude of the eigenvalues for the propagation matrix of a two component harmonic oscillator are plotted versus the outer time step Δt, where stability of the integrator is given by $|\lambda| \leqslant 1$. The two time periods are $T_1=2$ and $T_2=10$; the results are given for two inner time step values: Small $\Delta\tau=0.01$ (a), and large $\Delta\tau=0.6$ (b), close to the Verlet stability limit of $\Delta\tau_s=0.6366$. Resonances at multiples of the half fast period in the small $\Delta\tau$ limit are evident in (a), and the enhanced stability of PV in the large $\Delta\tau$ limit is indicated in (b).

$$k\Delta\tau \approx \frac{2m+1-\beta}{2}\left(\frac{2\pi}{\omega_1^{\text{eff}}}\right) = (2m+1+\beta)\frac{T_1^{\text{eff}}}{2}.$$

Thus, we see that instabilities appear for outer time steps near odd multiples of the fast (effective) half period in the small-time step limit. *This result is independent of α and holds for both PV and VV.*

Next we investigate the amplitude of the spikes for Case I $[\text{trace}(A_{\text{IV},*\text{V}}) < -2]$, noting again that a resonant time step is given by

$$k\theta \approx (2m+1+\beta)\pi \Rightarrow \cos(m\theta) \approx -1, \quad \sin(m\theta) \approx \beta\pi,$$

which implies

$$\text{trace}(A_{\text{IV}}) = 2\cos(k\theta) - 2k\alpha\,\sin(k\theta) \approx -2 - 2k\alpha\beta\pi.$$

The maximal eigenvalue is

$$r = \frac{\text{trace}(A_{\text{IV}}) - \sqrt{\text{trace}(A_{\text{IV}})^2 - 4}}{2}$$
$$\approx -1 - k\alpha\beta\pi - \sqrt{2k\alpha\beta\pi + (k\alpha\beta\pi)^2}$$
$$\approx -1 - 2k\alpha\beta\pi,$$

the last approximation is valid for large k. Since the nonresonant value of r is 1, the amplitudes of the resonant spikes behave like

$$|r| - 1 \approx 2k\alpha\beta\pi.$$

Since α is independent of k, and β increases only slightly with increasing k, the spike amplitudes increase almost linearly with k.

Next we examine the more interesting, large inner time step limit and take $\Delta\tau$ close to the single time step Verlet stability condition. Substituting Eq. (8) into Eqs. (17a) and (17b), we have

$$\alpha_{\text{VV}} \approx \frac{\epsilon^{-1/2}}{\sqrt{2}}(1-\epsilon)\frac{\lambda_2}{\lambda_1}, \quad \epsilon \ll 1 \tag{20}$$

$$\alpha_{\text{PV}} \approx \sqrt{2}\epsilon^{1/2}(1-\epsilon)\frac{\lambda_2}{\lambda_1}, \quad \epsilon \ll 1. \tag{21}$$

From Eqs. (19) and (10), the stability condition for VV scales as

$$k\alpha_{\text{VV}}\tan\left(\frac{k\theta}{2}\right) \approx k\epsilon^{-1/2}(1-\epsilon)\frac{\lambda_2}{\lambda_1}\tan\left(\frac{k}{2}\pi(2n+1) - k\frac{\sqrt{8}}{2}\epsilon^{1/2}\right) > 1, \quad n = 0,1,2,\cdots \tag{22}$$

and for PV as

$$k\alpha_{\text{PV}}\tan\left(\frac{k\theta}{2}\right) \approx k\epsilon^{1/2}(1-\epsilon)\frac{\lambda_2}{\lambda_1}\tan\left(\frac{k}{2}\pi(2n+1) - k\frac{\sqrt{8}}{2}\epsilon^{1/2}\right) > 1, \quad n = 0,1,2,\cdots. \tag{23}$$

For even integers k, we have $(k/2)\pi(2n+1+(\sqrt{8}/\pi)\epsilon^{1/2}) \approx m\pi^+$, $m=1,2,3,\ldots$, and

$$\tan\left(\frac{k}{2}\pi\left(2n+1+\frac{\sqrt{8}}{\pi}\epsilon^{1/2}\right)\right) \sim +\epsilon^{1/2}. \tag{24}$$

For odd integers k, we have $(k/2)\pi(2n+1+(\sqrt{8}/\pi)\epsilon^{1/2}) \approx (\pi/2)^+ + m\pi$, $m=0,1,2,\ldots$, and the scaling takes on the asymptotic form of

$$\tan\left(\frac{k}{2}\pi\left(2n+1+\frac{\sqrt{8}}{\pi}\epsilon^{1/2}\right)\right) \sim -\epsilon^{-1/2} + \mathcal{O}(\epsilon^{1/2}), \quad \text{for } \epsilon^{1/2} \ll 1. \tag{25}$$

By substituting Eq. (24) into Eqs. (22) and (23), we arrive at the following asymptotic behavior for PV and VV for even k:

$$\lim_{\Delta\tau\to\Delta\tau_s} k\alpha_{\text{VV}}\tan\left(\frac{k\theta}{2}\right) \sim +k\frac{\lambda_2}{\lambda_1}\epsilon^0,$$

$$\lim_{\Delta\tau\to\Delta\tau_s} k\alpha_{\mathrm{PV}} \tan\left(\frac{k\theta}{2}\right) \sim +k\frac{\lambda_2}{\lambda_1}\epsilon^1.$$

Similarly, substituting Eq. (25) into Eqs. (22) and (23), we find for odd k that

$$\lim_{\Delta\tau\to\Delta\tau_s} k\alpha_{\mathrm{VV}} \tan\left(\frac{k\theta}{2}\right) \sim -k\frac{\lambda_2}{\lambda_1}(\epsilon^{-1}+\mathcal{O}(\epsilon^0)),$$

$$\lim_{\Delta\tau\to\Delta\tau_s} k\alpha_{\mathrm{PV}} \tan\left(\frac{k\theta}{2}\right) \sim -k\frac{\lambda_2}{\lambda_1}(\epsilon^0+\mathcal{O}(\epsilon^1)).$$

These limits imply a negative value in the large $\Delta\tau$ limit and, therefore, do not contribute to the instability.

Recall that the instability condition holds for values of $k\alpha \tan(k\theta/2)>1$. In the large $\Delta\tau$ limit, we have only even k values contributing to the instability; $k\alpha \tan(k\theta/2)$ scales $\sim\epsilon^0$ for VV and *decays* like ϵ^1 for PV. Therefore, we have an interesting stabilizing effect for the PV scheme in the large $\Delta\tau$ limit: Stability may be maintained around the resonant regions as well, i.e., if the value of $k(\lambda_2/\lambda_1)$ or ϵ is small enough (noting that $\lambda_2/\lambda_1<1$). In the case of PV, we have a boundary region (layer) where the stability of the outer time step can increase as we approach the large $\Delta\tau$ limit, i.e., $k_{\mathrm{unstable}}(\mathrm{PV})\sim(\lambda_1/\lambda_2)\epsilon^{-1}$. This is in contrast to VV where stability is solely a function of λ_1/λ_2, $k_{\mathrm{unstable}}(\mathrm{VV})\neq k(\epsilon)$, i.e., $k_{\mathrm{unstable}}(\mathrm{VV})\sim\lambda_1/\lambda_2$.

In Fig. 3 we present the function $k\alpha \tan(k\theta/2)$ for the PV and VV integrators where the two time periods are $T_1=2$ and $T_2=10$. We use a modest inner time step of $\Delta\tau=0.4$ and an inner time step $\Delta\tau=0.6$ close to the Verlet stability limit of $\Delta\tau_s=0.6366$. The approximately equivalent stability behavior for small to modest $\Delta\tau$ is contrasted to the different results for $\Delta\tau$ approaching the Verlet stability limit.

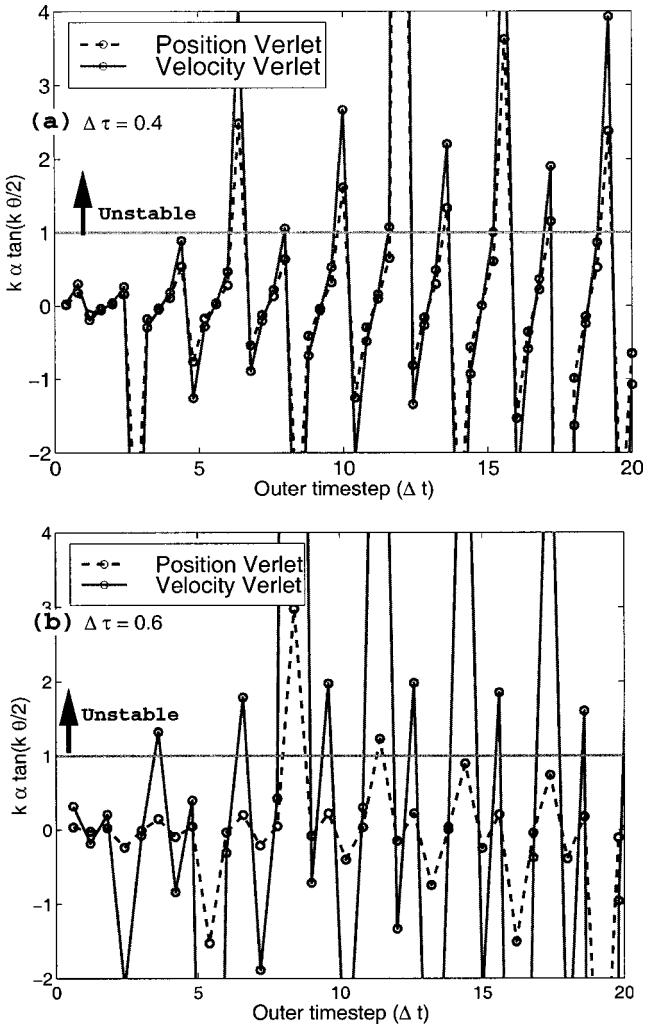

FIG. 3. The stability condition of $k\alpha \tan(k\theta/2)\leqslant 1$ for Case I is plotted for the position-Verlet and velocity-Verlet integrators. The two time periods are $T_1=2$ and $T_2=10$; the results are given for two inner time steps: $\Delta\tau=0.4$ and 0.6, the latter close to the Verlet stability limit of $\Delta\tau_s=0.6366$. The approximately equivalent stability conditions found for small to moderate $\Delta\tau$ are contrasted to an enhanced stability shown for PV in the limiting values of large $\Delta\tau$.

2. Case II: trace($A_{IV,*V}$)>2

The condition $\mathrm{trace}(A_{\mathrm{IV},*\mathrm{V}})>2$ is equivalent to

$$-1+\cos(k\theta)-k\alpha\sin(k\theta)$$
$$=-2\sin^2\left(\frac{k\theta}{2}\right)-2k\alpha\sin\left(\frac{k\theta}{2}\right)\cos\left(\frac{k\theta}{2}\right)>0,$$

and states that an instability will occur for

$$-k\alpha<\tan\left(\frac{k\theta}{2}\right)<0$$

or

$$-1<\frac{1}{k\alpha}\tan\left(\frac{k\theta}{2}\right)<0. \tag{26}$$

The second bound $[\tan(k\theta/2)<0]$ results from the fact that the inequality can only be achieved if $\sin(k\theta/2)\cos(k\theta/2)<0$, i.e., $\tan(k\theta/2)<0$; this limit is a strong boundary in the large $k\alpha$ limit.

To examine the stability condition of Case II in the large $\Delta\tau$ limit, we apply the same asymptotic results found in Case I above. For VV we utilize Eqs. (20) and (10) to arrive at

$$\frac{1}{k\alpha_{\mathrm{VV}}}\tan\left(\frac{k\theta}{2}\right)\approx\frac{\epsilon^{1/2}}{k(1-\epsilon)}\frac{\lambda_1}{\lambda_2}\tan\left(\frac{k}{2}\pi(2n+1)+k\frac{\sqrt{8}}{2}\epsilon^{1/2}\right),\quad n=0,1,2,\cdots.$$

For PV, we use Eqs. (21) and (10) to arrive at

$$\frac{1}{k\alpha_{\mathrm{PV}}}\tan\left(\frac{k\theta}{2}\right)\approx\frac{\epsilon^{-1/2}}{k(1-\epsilon)}\frac{\lambda_1}{\lambda_2}\tan\left(\frac{k}{2}\pi(2n+1)+k\frac{\sqrt{8}}{2}\epsilon^{1/2}\right),\quad n=0,1,2,\cdots. \tag{27}$$

Again, for even values of k we have

$$\tan\left(\frac{k}{2}\pi\left(2n+1+\frac{\sqrt{8}}{\pi}\epsilon^{1/2}\right)\right)\sim+\epsilon^{1/2},$$

and for odd values of k we have

$$\tan\left(\frac{k}{2}\pi\left(2n+1+\frac{\sqrt{8}}{\pi}\epsilon^{1/2}\right)\right)\sim-\epsilon^{-1/2}+\mathcal{O}(\epsilon^{1/2}),$$

$$\text{for } \epsilon^{1/2}\ll 1. \tag{28}$$

These results lead to the asymptotic behavior for VV and PV with even k as

$$\lim_{\Delta\tau\to\Delta\tau_s}\frac{1}{k\alpha_{\mathrm{VV}}}\tan\left(\frac{k\theta}{2}\right)\sim+k^{-1}\frac{\lambda_1}{\lambda_2}\epsilon^1,$$

$$\lim_{\Delta\tau\to\Delta\tau_s}\frac{1}{k\alpha_{\mathrm{PV}}}\tan\left(\frac{k\theta}{2}\right)\sim+k^{-1}\frac{\lambda_1}{\lambda_2}\epsilon^0.$$

Around possible resonant cases of odd $k=1,3,5,\ldots$, we have

$$\lim_{\Delta\tau\to\Delta\tau_s}\frac{1}{k\alpha_{\mathrm{VV}}}\tan\left(\frac{k\theta}{2}\right)\sim-k^{-1}\frac{\lambda_1}{\lambda_2}(\epsilon^0+\mathcal{O}(\epsilon^1)), \tag{29}$$

$$\lim_{\Delta\tau\to\Delta\tau_s}\frac{1}{k\alpha_{\mathrm{PV}}}\tan\left(\frac{k\theta}{2}\right)\sim-k^{-1}\frac{\lambda_1}{\lambda_2}(\epsilon^{-1}+\mathcal{O}(\epsilon^0)). \tag{30}$$

For even k, the positive asymptotic result does not contribute to the instability. For odd k values, we again see a favorable analysis for PV. Here instability occurs for small negative values of $(1/k\alpha)\tan(k\theta/2)$. The VV analysis has negative values of $(1/k\alpha)\tan(k\theta/2)$ which are independent of ϵ to first order, i.e., $(1/k\alpha)\tan(k\theta/2)$ approaches a constant value in the large $\Delta\tau$ limit. For PV, the negative values of $(1/k\alpha)\tan(k\theta/2)$ are *increasing* as ϵ^{-1}. Therefore, we again have an interesting stabilizing effect for the PV scheme in the large $\Delta\tau$ limit: Stability may be maintained around the resonant regions as long as the value of $(k^{-1})\lambda_1/\lambda_2$ is *large* enough (noting that $\lambda_1/\lambda_2>1$) or ϵ is small enough. We subsequently arrive at the same results found in Case I, namely, for PV (here for odd k) the stability of the outer time step can increase as we approach the large $\Delta\tau$ limit, i.e., $k_{\mathrm{unstable}}(\mathrm{PV})\sim(\lambda_1/\lambda_2)\epsilon^{-1}$; $k_{\mathrm{unstable}}(\mathrm{PV})$ will increase with decreasing ϵ. For VV, the maximal stability value is solely a function of λ_1/λ_2.

In Fig. 4, we present the function $(1/k\alpha)\tan(k\theta/2)$ for the PV and VV integrators where the two time periods are $T_1=2$ and $T_2=10$. The results are given for a moderate inner time step of $\Delta\tau=0.4$ and a larger value $\Delta\tau=0.6$ close to the Verlet stability limit of $\Delta\tau_s=0.6366$. Approximately equivalent stability conditions are found for small to moderate $\Delta\tau$; for $\Delta\tau$ near $\Delta\tau_s$, an enhanced stability is found in the outer time step for PV.

To examine the size of the resonant spikes, i.e., the distance of the eigenvalues from the unit circle, we note that Eq. (27) implies

$$\frac{k\theta}{2}\approx(m-\beta)\pi,\quad 0<\beta<\frac{1}{2}.$$

In the small inner-time step limit, we obtain

$$k\Delta\tau\approx(m-\beta)T_1^{\mathrm{eff}}.$$

We find that the instability appears for outer time steps near integer multiples of the effective fast period.

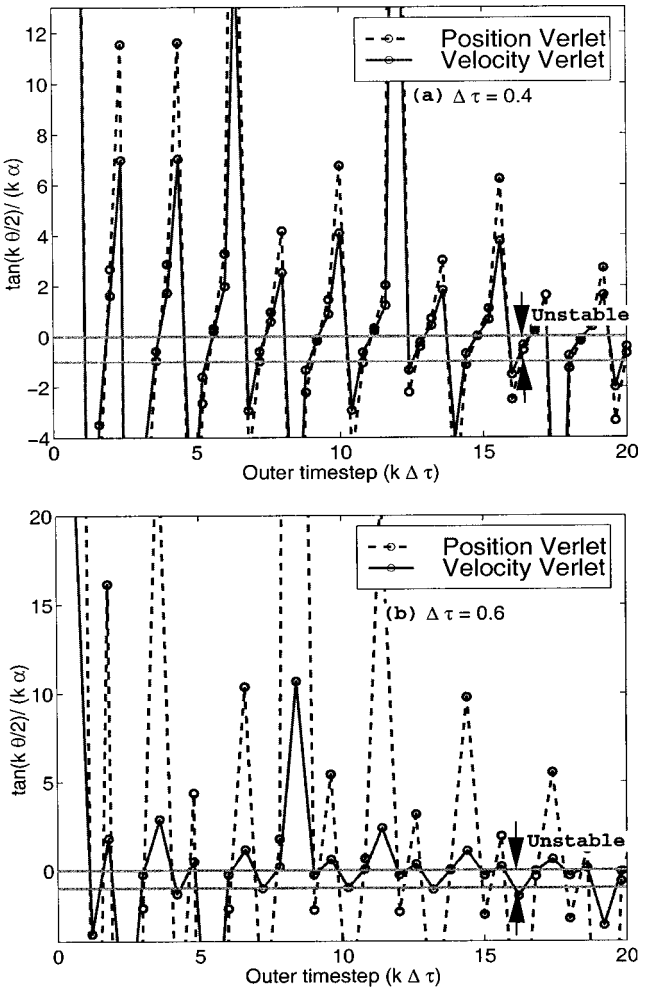

FIG. 4. The stability condition of $\tan(k\theta/2)/(k\alpha)\geqslant 1$ for Case II is plotted for the position-Verlet and velocity-Verlet integrators. The two time periods are $T_1=2$ and $T_2=10$; the results are given for two inner time steps: $\Delta\tau=0.4$ and 0.6, the latter close to the Verlet stability limit of $\Delta\tau_s=0.6366$. The Verlet integrator is shown to be unstable for all small Δt when $\Delta\tau$ approaches the inner time step stability condition.

To approximate the spike amplitudes for Case II, we note that near the resonance

$$k\theta\approx(2m-1)\pi\Rightarrow\cos(k\theta)\approx 1,\ \sin(k\theta)\approx-\beta\pi.$$

With a similar analysis presented for Case I above, we find that the increasing spike height is linear with k, for large k

$$|r|-1\approx k\alpha\beta\pi.$$

In both cases, the amplitude of the resonant spikes scales to leading order, in the large k limit [or more formally $(k\alpha\beta)\gg 1$], as

$$ampl\approx k\alpha\beta\pi, \tag{31}$$

where β is a small positive number, $0<\beta<1/2$. By substituting Eqs. (17a) and (17b) into Eq. (31) and taking the ratio of the two results, we find that the approximate amplitude of the "resonant spikes" is always smaller for the PV formulation. That is

$$\frac{ampl_{\mathrm{PV}}}{ampl_{\mathrm{VV}}}\approx 1-\frac{\Delta\tau^2}{4}\lambda_1, \tag{32}$$

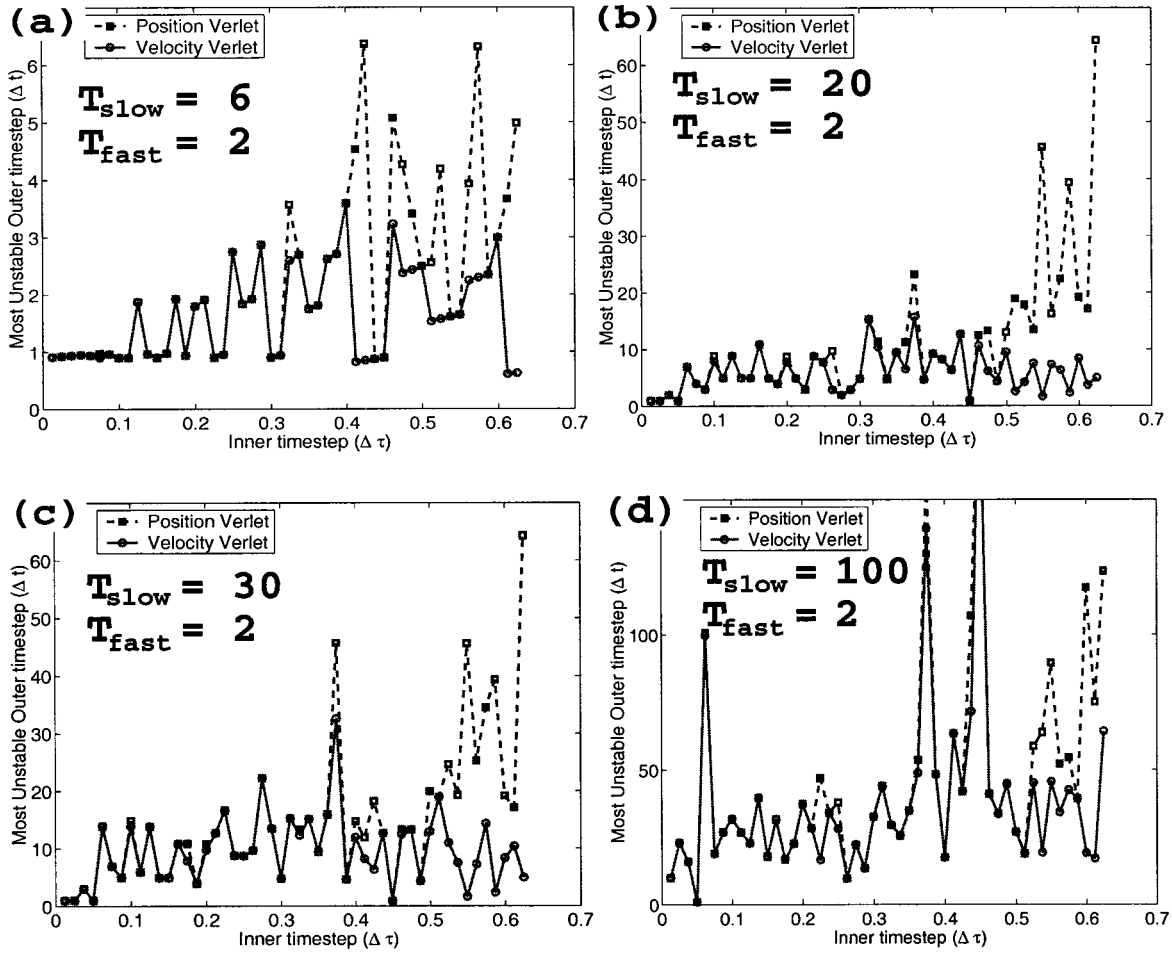

FIG. 5. The outer time step stability limit as calculated from the analysis of the propagation matrix for both the position-Verlet and velocity-Verlet integrators. The results are presented for various inner time steps up to the Verlet stability limit of $\Delta\tau_s = 0.6366$. Various time scale separations are examined in (a)–(d): $(T_1, T_2) = (2, 6)$, $(2, 20)$, $(2, 30)$, and $(2, 100)$. PV allows larger outer time steps Δt than VV as $\Delta\tau_s$ is approached.

this result holds for Case I as well. Furthermore, if we examine the large inner-time step limit and take $\Delta\tau$ close to the single-time step Verlet stability condition, Eq. (8), we have

$$\frac{ampl_{\mathrm{PV}}}{ampl_{\mathrm{VV}}} \approx 2\epsilon,$$

for

$$\Delta\tau = 2(1-\epsilon)/\sqrt{\lambda_1}, \quad \epsilon \ll 1.$$

This limiting behavior also holds for Case I. In the limit of small inner time steps, the resonant effects are similar for the PV and VV formulations, as confirmed from Eq. (32) and through stability calculations of the impulse-Verlet propagation matrix ($A_{\mathrm{IV},*\mathrm{V}}$) [Eq. (12)].

Lastly, we examine the stability boundary for two cases where the slow and fast periods have relative ratios of 3, 10, 15, and 50. The outer time step stability limit is calculated from the analysis of the propagation matrix for both the PV and VV integrators. The results are presented for various inner time steps up to the Verlet stability limit. The most unstable outer time step is defined as the first value of k that meets the instability condition, $\mathrm{trace}(A_{\mathrm{IV},*\mathrm{V}}) < -2$ or $\mathrm{trace}(A_{\mathrm{IV},*\mathrm{V}}) > 2$, for a given $\Delta\tau$. Figure 5 plots the most unstable outer time step, as a function of $\Delta\tau$. The four time scale separations used are $(T_1, T_2) = (2, 6)$, $(2, 10)$, $(2, 20)$, and $(2,100)$. For PV, the stability region that scales as $k \sim \epsilon^{-1}$ at the large $\Delta\tau$ limit ($\Delta\tau_s = 0.6366$) is illustrated.

III. BIOMOLECULAR SIMULATION

The results above suggest that PV is preferable to VV in impulse splitting schemes, particularly at larger inner time steps. This conclusion supports observations made in Ref. 15, and noted in Ref. 13, that PV has better stability in terms of amplitude of root-mean-square (rms) fluctuations in the total energy for nonlinear biomolecular systems. Here we present an application of our algorithms in Ref. 15 for a solvated protein system with ~14 000 atoms. The integration is based on a three-level splitting scheme and incorporates the particle-mesh Ewald (PME) scheme for electrostatic evaluations.[27,28]

Several different strategies can be used for implementing the three-level force splitting as discussed above. We take the Ewald reciprocal force as the long-range "slow" force, the bonded terms in the fast force class, and all other terms in the medium class force. This is a typical force splitting used in rigid-cutoff methods that use switching functions to define

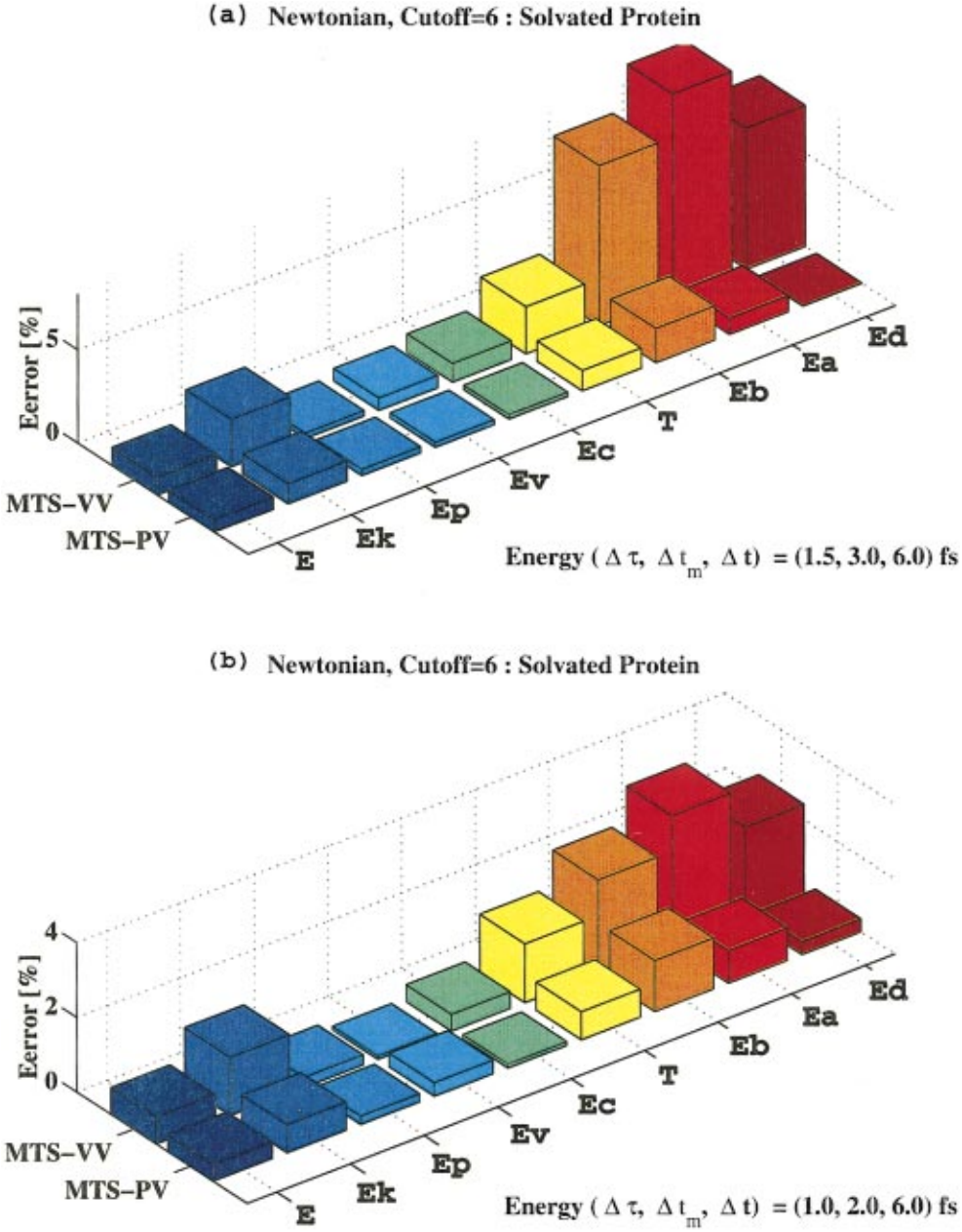

FIG. 6. (Color) The deviation in energy components relative to the baseline STS-PV integrator for the solvated protein system are compared for MTS-VV and MTS-PV at two time step combinations. Here the total energy (E) and its components, kinetic energy (Ek), potential energy (Ep), van der Waals energy (Ev), electrostatic energy (Ec), bond energy (Eb), bond angle energy (Ea), and dihedral energy (Ed) are plotted along with the temperature (T) percent differences. A cutoff of 6 Å and time steps of $(\Delta\tau,\Delta t_m,\Delta t)=(1.5, 3.0, 6.0)$ fs and (1.0, 2.0, 6.0) fs are used in (a) and (b), respectively. Larger relative errors are found for the velocity-Verlet formulation and these errors tend to increase with increasing medium time step; this contrast/behavior of position-Verlet, which maintains a comparatively constant error with an increased medium time step. Total integration lengths in all simulations were 300 ps.

slow forces.[6,16] The medium force evaluation includes 1–4 interaction, van der Waals terms, and the real space sum for the PME method; the neighbor exclusion correction term for the real space sum was updated at each medium term evaluation. Nonbonded (NB) list-management routines were applied at each medium force call; the AMBER software includes tests to determine if the NB list utilities should be invoked.

An interesting aspect of the numerical integration, as discussed in Ref. 15, is that the Ewald sum does not completely separate the time scales of the electrostatic term. Thus, fast force components exist within the slow force (reciprocal term) component. In an effort to separate the time scales of the electrostatic force component, we suggest[29] a modified Ewald-type core function that effectively splits the lattice sum and formulates the reciprocal space potential and real space sum into isolated far-field and near-field interactions, respectively.

In Fig. 6 we present the error in mean energy components for a Newtonian integration of the solvated protein; comparisons to an accurate $\Delta t=0.5$ fs single-time step integration are made. The effective Ewald cutoff was 6 Å, and time steps of $(\Delta\tau,\Delta t_m,\Delta t)=(1.5, 3.0, 6.0)$ fs and (1.0, 2.0, 6.0) fs were used for both PV and VV; total integration

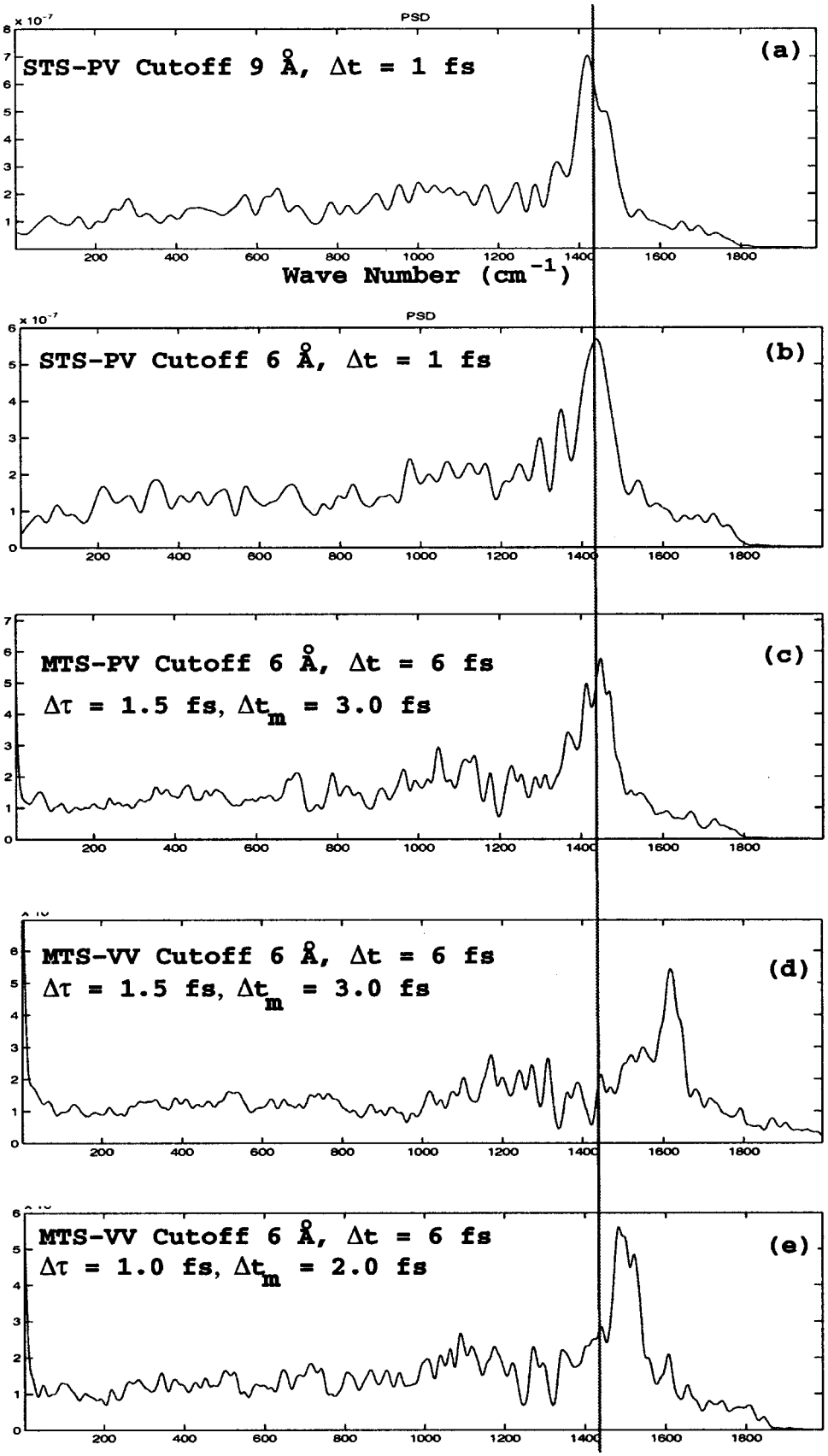

FIG. 7. The discrete Fourier transforms of the velocity autocorrelation function of the solvated protein simulation for 300 ps MTS simulations are compared to a 40 ps STS-PV simulations ($\Delta t = 1$ fs and cut-off values for 6 and 9 Å). Three MTS protocols with a cut-off value of 6 Å are used in (c)–(e): Time steps of $(\Delta\tau, \Delta t_m, \Delta t) = (1.5, 3.0, 6.0)$ fs for PV, time steps of $(\Delta\tau, \Delta t_m, \Delta t) = (1.5, 3.0, 6.0)$ fs for VV, and time steps of (1.0, 2.0, 6.0) fs for VV.

lengths were 300 ps. Extensive numerical experiments (see Ref. 15) indicate that an outer time step of $\Delta t < 6$ fs is required to ensure stable long-time trajectories. For an acceptance criteria, a threshold of less than 5% deviation from the baseline STS in the energy component is typical, indicating that the ($\Delta t_m = 3$ fs, $\Delta t = 6$ fs) MTS-PV result is allowable but the MTS-VV is not. For the smaller medium time step of ($\Delta t_m = 2$ fs, $\Delta t = 6$ fs), both MTS-PV and MTS-VV have

acceptable errors; however, the PV errors are lower by a factor of 2 or more.

In general, larger relative errors are found for the VV formulation and these errors tend to increase with increasing medium time step, as opposed to the PV formulation which maintains a comparatively constant error with an increased medium time step. VV tends to introduce large error in the bonded ''fast'' components and significantly influences the kinetic-energy component as well. In Ref. 15, an additional comparison was presented for the MTS integration where modest Langevin forces are used to stabilize the integration up to $\Delta t = 8.0$ fs. The Langevin results were in general agreement with the Newtonian results, where the largest errors are found in the bonded and kinetic-energy components.

Lastly, we analyze the spectrum of the discrete Fourier transform of the velocity autocorrelation of the solvated protein simulation for the Newtonian MTS ($\Delta t = 6.0$ fs) simulations for both PV and VV. In Fig. 7(c), we plot the spectra for the MTS-PV simulation with a cut-off value of 6 Å and time steps of $(\Delta\tau, \Delta t_m, \Delta t) = (1.5, 3.0, 6.0)$ fs. The Newtonian MTS-VV simulation with a cut-off value of 6 Å and time steps of $(\Delta\tau, \Delta t_m, \Delta t) = (1.5, 3.0, 6.0)$ fs and (1.0, 2.0, 6.0) fs are plotted in Figs. 7(d) and 7(e). The Newtonian STS results for $\Delta t = 1$ fs and cut-off values of 6 and 9 Å are also presented for comparison. The spectrum of the MTS-PV simulation is in good agreement with the STS results, and the spectral peak appears at ~ 1450 cm^{-1}. However, the MTS-VV results do not accurately capture this spectral peak. The part of the spectrum below 2000 cm^{-1} originates from bond stretching of the heavier atoms (e.g., C–O). The MTS-VV results indicate an upward drift in the lower 2000 cm^{-1} components with respect to increased Δt_m at this relatively large Δt; Cheng and Merz[30] found similar results in the drift of the spectra for their MTS-VV RESPA integrator.

IV. SUMMARY

Our numerical analysis confirms that the position-Verlet formulation for multiple-time-step integrations has an advantage over the velocity-Verlet formulation in the large time step limit. Namely, better numerical behavior for position-Verlet results when the inner time step approaches its Verlet stability limit. Another observation is that the eigenvalues of propagation matrix for position-Verlet generally have a relatively small deviation from the unit circle, even for large unstable time steps, for a simple model harmonic problem. This suggests a possible explanation for the large stable outer time steps associated with the MTS-LN protocol, which is a slight modification to the position-Verlet protocol. The LN protocol uses a midpoint extrapolation of the medium-class force, as well as modest Langevin damping to stabilize energy drifts and damps resonances.

Our theoretical analysis suggests that resonant-type instabilities can be alleviated for the position-Verlet protocol, when the inner time step approaches its Verlet stability limit from below. Such enhanced stability near the large inner-time step limit, and the general result that the magnitude of the eigenvalues of position-Verlet's propagation remain close to the unit circle, suggest that PV-based schemes are good starting points for future algorithm development; the LN protocol[6] is one such direction. For biomolecular-dynamic simulations, the long-time integrations necessary to sample the wide range of possible conformations remain a formidable challenge. The use of large inner time steps, though possibly associated with larger numerical errors, may be an acceptable compromise between accuracy and long-time trajectories.

ACKNOWLEDGMENTS

The work is supported by NSF award ASC-9318159, NIH award R01 GM55164, and a John Simon Guggenheim fellowship to one of the authors (T.S.) an investigator of the Howard Hughes Medical Institute.

[1] M. P. Allen and D. J. Tildesley, *Computer Simulations of Liquids* (Oxford University Press, Oxford, 1989).
[2] T. Schlick, in *Lecture Notes in Computational Science and Engineering* (Springer-Verlag, Berlin/New York, 1998).
[3] T. Schlick, Structure **9**, R45 (2001).
[4] A. Sandu and T. Schlick, J. Comput. Phys. **151**, 74 (1999).
[5] T. Schlick, E. Barth, and M. Mandziuk, Annu. Rev. Biophys. Biomol. Struct. **26**, 181 (1997).
[6] T. Schlick and E. Barth, J. Chem. Phys. **109**, 1617 (1998).
[7] J. J. Biesiadecki and R. D. Skeel, J. Comput. Phys. **109**, 318 (1993).
[8] H. Grubmuller, H. Heller, A. Windemuth, and K. Schulten, Mol. Simul. **6**, 121 (1991).
[9] D. D. Humphreys, R. A. Friesner, and B. J. Berne, J. Phys. Chem. **98**, 6885 (1994).
[10] J. A. Izaguirre, S. Reich, and R. D. Skeel, J. Phys. Chem. **110**, 9853 (1999).
[11] B. Garcia-Archilla, J. M. Sanz-Serna, and R. D. Skeel, SIAM J. Sci. Comput. (USA) **20**, 930 (1998).
[12] M. E. Tuckerman, B. J. Berne, and G. J. Martyna, J. Chem. Phys. **94**, 6811 (1991).
[13] M. E. Tuckerman, B. J. Berne, and G. J. Martyna, J. Chem. Phys. **97**, 1990 (1992).
[14] M. Watanabe and M. Karplus, J. Chem. Phys. **99**, 8063 (1993).
[15] P. F. Batcho, D. A. Case, and T. Schlick J. Chem. Phys. **115**, 4003 (2001), preceding paper.
[16] E. Barth and T. Schlick, J. Chem. Phys. **109**, 1633 (1998).
[17] T. Schlick, J. Comput. Phys. **151**, 1 (1999).
[18] T. Schlick, A. T. Brunger, L. V. Kale, J. A. Board, Jr., J. Hermans, and K. Schulten, J. Comput. Phys. **151**, 9 (1999).
[19] T. E. Cheatham, III and B. R. Brooks, Theor. Chem. Acc. **99**, 279 (1999).
[20] D. Strahs and T. Schlick, J. Mol. Biol. **301**, 643 (2000).
[21] W. D. Cornell, P. Cieplak, C. I. Bayly *et al.*, J. Am. Chem. Soc. **117**, 5179 (1995).
[22] D. A. Pearlman, D. A. Case, J. W. Caldwell, W. S. Ross, R. E. Cheatman, S. DeBolt, D. Ferguson, G. Seibel, and P. Kollman, Comput. Phys. Chem. **91**, 1 (1995).
[23] G. Zhang and T. Schlick, J. Comput. Chem. **14**, 1212 (1993).
[24] G. Zhang and T. Schlick, J. Chem. Phys. **101**, 4995 (1994).
[25] T. Schlick, R. D. Skeel, M. Mandziuk, and K. Srinivas, J. Comput. Phys. **140**, 1 (1998).
[26] R. D. Skeel and K. Srinivas, SIAM J. Num. Anal. **38**, 129 (2000).
[27] U. Essmann, L. Perera, M. L. Berkowitz, T. Darden, H. Lee, and L. G. Pedersen, J. Chem. Phys. **103**, 8577 (1995).
[28] T. Darden, D. York, and L. Pedersen, J. Chem. Phys. **98**, 10089 (1993).
[29] P. F. Batcho and T. Schlick (unpublished).
[30] A. Cheng and K. M. Merz, Jr., J. Phys. Chem. B **103**, 5396 (1999).